Annals of Biomedical Engineering, Vol. 31, pp. 363–373, 2003
Printed in the USA. All rights reserved.

0090-6964/2003/31(4)/363/11/$20.00

Relation Between Structure, Function, and Imaging in a Three-Dimensional Model of the Lung

NORA T. TGAVALEKOS,[1] J. G. VENEGAS,[2] B. SUKI,[1] and K. R. LUTCHEN[1]

[1]Department of Biomedical Engineering, Boston University, Boston, MA and [2]Department of Anesthesia, and Critical Care, Massachusetts General Hospital, Boston, MA

(Received 20 August 2002; accepted 27 December 2002)

Abstract—Previous studies have reported morphometric models to predict function relations in the lung. These models, however, are not anatomically explicit. We have advanced a three-dimensional airway tree model to relate dynamic lung function to alterations in structure, particularly when constriction patterns are imposed heterogeneously in specific anatomic locations. First, we predicted the sensitivity of dynamic lung resistance and elastance (R_L and E_L) to explicit forms of potential constriction patterns. Simulations show that severe and heterogeneous peripheral airway constriction confined to a single region in the lung (apex, mid, or base) will not produce substantial alterations in whole lung properties as measured from the airway opening. Conversely, when measured R_L and E_L are abnormal, it is likely that significant (but not necessarily homogeneous) constriction has occurred throughout the entire airway tree. We also introduce the concept of image-assisted modeling. Here positron emission tomographic imaging data sensitive to ventilation heterogeneity is synthesized with R_L and E_L data to help identify which airway constriction conditions could be consistent with both data sets. An ultimate goal would be personalized predictions. © *2003 Biomedical Engineering Society.* [DOI: 10.1114/1.1557972]

Keywords—Asthma, Airway hyperresponsiveness, Ventilation distribution, PET.

INTRODUCTION

Rapid advances in computational modeling of the lung have led to fundamental new understandings of how lung morphometry, anatomy, and biomechanical properties impact lung function. Morphometric models were initiated by Weibel *et al.*,[21] who assigned lengths and diameters to a symmetrical airway tree based on measurements of human airway casts. A more realistic model by Horsfield[6,5] is asymmetric and assigns lengths, diameters, and recursion indices to each order in the airway tree. This model retains the mean distribution of airway properties as they exist in real lungs. The recursion indices define the degree of asymmetry in the tree.

Address correspondence to Kenneth R. Lutchen, PhD, Department of Biomedical Engineering, Boston University, 44 Cummington St., Boston, MA 02215. Electronic mail: klutch@bu.edu

Several studies advanced these morphometric models to predict function. For example, Thorpe and Bates,[19] using the Horsfield ordering system for a dog lung, investigated the impact of heterogeneous airway smooth muscle (ASM) constriction on dynamic resistance (R_L) and elastance (E_L). Recently, Lutchen and colleagues[2,3,12] advanced previous Horsfield models to include airway wall properties and alveolar tissue elements. Their studies explored the frequency dependence of R_L and E_L after heterogeneous bronchoconstriction[12] and ASM shortening[2] were imposed on the airways. These studies predicted that the pattern of constriction should be a crucial component of the asthma diseased phenotype. In particular, there would be a substantial increase in R_L and E_L especially at typical breathing rates even if only a small (~10%) fraction of the peripheral airways was highly constricted, so long as they were randomly distributed throughout the lung. Such a constriction pattern would impose difficulties in both the mechanics of breathing[2] and in ventilation distribution.[3] Experimental evidence for these types of heterogeneities has subsequently been reported using either measurements of dynamic mechanical properties[11] or from imaging data sensitive to ventilation distribution.[1,10]

While these previous computational studies have employed models with structures that are consistent with the morphological and statistical features of the airway tree, the models have not been anatomically explicit. That is, there is not a one to one correlation between the airway tree and the real anatomy such as specific lobes or airways in the thoracic cage. Hence, with a morphometric model one could probe questions such as: ''Which size airways need to be constricted and by how much to produce clinically important changes in lung function?''. But, with an anatomically consistent model, one could further ask ''Which airway locations (not just sizes) need to be constricted in order to produce important changes in mechanical and ventilation lung function?''. With continuous improvement in imaging modalities, it is becoming increasingly possible to establish precise physical

locations and degrees of structural or functional defects in the lung during disease. Such data will beg the question of how explicit anatomic defects alter function.

In 1999, Kitaoka *et al.* created three-dimensional (3D) space filling airway tree models in which the airways correspond to a specific physical location in the tree.[8] A similar 3D model of a host-shape dependent conducting airway tree model was generated by Tawhai in 2000.[18] These models are capable of capturing the sensitivity of anatomic geometry to changes in the terminal branch flow, or branching angle. However, the 3D models only described the geometry of the tree and have not yet been used to predict changes in function when explicit anatomic constrictions have been imposed on the lung.

In this paper, we have advanced a 3D airway tree model to predict function from structure particularly when constriction patterns are imposed heterogeneously on the tree in specific anatomic locations. We also introduce the notion of image assisted modeling by providing a framework for synthesizing this modeling approach with positron emission tomographic (PET) imaging data sensitive to ventilation distribution heterogeneity.

METHODS

We used the 3D airway tree model of Kitaoka *et al.*[8] This airway tree model utilizes a deterministic space-filling algorithm to create a branching structure, which is physiologically consistent in the amount of fluid delivered to the terminal airways and the spatial arrangement of branches within the lung. Briefly, the algorithm specifies internal and external boundaries that outline anatomical contours such as the aorta, thoracic cage, and heart. These contours establish an outline of a realistic human lung. The model assumes dichotomous branching. Fluid flow before branching is conserved such that the sum of the flow moving into the daughter branches (Q_1 and Q_2) is equivalent to the flow in the parent branch (Q_p):

$$Q_p = Q_1 + Q_2 . \tag{1}$$

The diameter of each airway is computed by applying the relationship described by Murray,[15] in which fluid flow through a circular rigid tube is related to the diameter of the tube

$$Q = C d^n , \tag{2}$$

where Q is the fluid flow rate, d is the diameter, C is a constant specific to the organ and fluid, and n is the diameter exponent.[14] The flow-dividing ratio, r, is a random variable, which ranges between 0 and 0.5 and creates asymmetry in the branching as

$$d_1 = d_p r^{1/n}, \qquad d_2 = d_p (1-r)^{1/n}. \tag{3}$$

The length of each branch is defined to be equal to three times the diameter.[8]

The fluid flow rate (Q_p), and the location of the trachea are initially specified. The model also designates the location of the main lobular bronchi. Starting from the trachea, branching along a pathway continues until one of the following conditions is met: (1) The flow in the daughter branch decreases below a flow rate threshold, which is initially specified and based on the condition that gas transport changes from conduction to diffusion in the terminal branches of the tree; and (2) the daughter branch extends beyond the boundary region.[8]

A base line human airway tree structure with a total of 50,400 branches with 28 distinct airway generations was created using the Kitaoka algorithm. A generation is defined as all airways occurring at a specific number of bifurcations from the trachea. The trachea is designated generation 1 and the terminal airways can occur as early as the eighth generations or as late as the 28th. The distribution of total number of branches that exist at a given generation is Gaussian-like, with the most number occurring at generation 16 [Fig. 1(A)]. Due to random variations in flow distribution, each generation has a distribution of diameters and lengths [Fig. 1(B)]. Each segment has 3D coordinates specifying the 3D location.

Calculation of Function in 3D Lung Model

Impedance of a single airway is calculated using an acoustic transmission line model, which takes into account resistive (R) and inertial (I) forces as in Ref. 12. Each airway includes a shunt gas compliance and a shunt airway wall impedance modeled as a parallel combination of soft tissue and cartilage.[17] The mechanical properties of the airway wall are a function of airway diameter and airway wall thickness. The airway walls are divided into three layers: adventitia, smooth muscle, and submucosa. Wall thicknesses are based on the histological measurements of human airway walls described by Kuwano *et al.*[9] The wall thicknesses are diameter dependent and account for variations in healthy and asthmatic wall properties.[2] Attached to each terminal airway is an alveolar tissue element, which is composed of a gas compression compliance and viscoelastic tissue model. The viscoelastic tissue model is a constant phase model.[4] Specifically, from the literature on healthy human lungs we applied a total tissue viscance (G) of 1.22 cm H_2O/I/s and a tissue elastance (H) of 5.8 cm H_2O/I. We also assumed a total lung volume at FRC of 3 L. Lung tissue

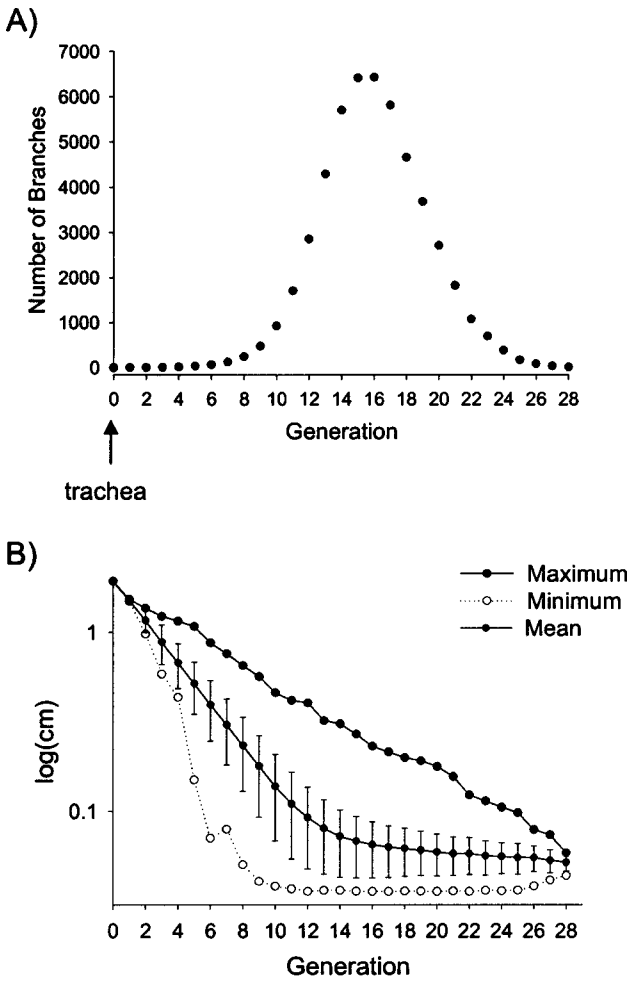

FIGURE 1. (A) Distribution of the number of branches in each generation of the airway tree. Each branch has a unique diameter, length and location in the tree. (B) Maximum, minimum, and mean diameters of the branches in each generation.

properties and total alveolar volume was distributed uniformly to the alveolar-tissue elements attached to the terminal airways.

The manner in which the 3D airway tree is traversed for computing R_L and E_L is discussed in detail in the Appendix. In general, an airway tree file is created such that the each file entry contains the properties of a branch, i.e., generation number, diameter, and length. The first entry is always the trachea and each subsequent entry is the left daughter of the previous entry. We take advantage of this setup to compute the input impedance (Z_{in}) of the entire airway tree structure. Z_{in} is the impedance looking into the trachea and includes the parallel/series combination of all subtending airway branches. Previous methods of traversing through an asymmetrical bifurcating tree to calculate Z_{in} have taken advantage of a stack based computational algorithm because of the book keeping and memory demands resulting from imposing heterogeneous constriction patterns.[12] We have modified the stack-based algorithm to traverse through the 3D tree, and are able to treat each branch individually so that heterogeneous constriction patterns may be imposed on the 3D tree. Also, since we will compare simulations to real data, we need to account for the upper (extrathoracic) airways not included in the 3D airway tree. Here we add an upper airway resistance, $R_{uaw}=2.0$ cm H_2O/l/s. This value is equivalent to the difference between total airway resistance[13] and simulated base line airway tree resistance, in series with the trachea. All simulations (baseline included) have the R_{uaw} incorporated. To impose constriction in the lung we first identify a specific anatomic location to be constricted (e.g., upper right lobe). For each selected airway in this region, a random draw is performed on a Gaussian distribution function with a given mean (μ) and standard deviation (SD). The degree of heterogeneity in constriction is determined by the value of the SD. For each preselected airway, the random draw will return a constriction factor, which will alter the baseline diameter.

Simulation Studies

The focus of these studies was to advance a 3D lung model to predict the impact on function when anatomically explicit heterogeneous structural changes are imposed on the entire lung. Simulations were performed at FRC and diameter and lengths were scaled from TLC using a sigmoidal scaling function.[12] R_L and E_L were simulated from 0.1 to 8.0 Hz for varying degrees and locations of constriction.

Four sets of simulation studies were performed. The first three examined the sensitivity of whole lung mechanics to constriction patterns placed in either explicit anatomic locations or distributed throughout the lung in a prescribed apex-to-base fashion. The fourth study was data driven and intended to introduce the concept of image-assisted modeling with an eventual goal to establish the types of constriction patterns that may or may not be occurring in an individual's lungs.

The first study examined the sensitivity of the predicted R_L and E_L to the stochastic nature of the airway tree as created when applying a probabilistic constriction pattern. Specifically, we imposed a Gaussian distributed constriction to all the peripheral airways with a μ constriction of 50% and SD of 70%. A Monte Carlo analysis of 20 runs was performed by simulating R_L and E_L from 0.1 to 8 Hz after creating a distinct set of 20 random draws from the Gaussian constriction probability distribution function (i.e., 20 distinct constricted airway trees, each drawn from the same distribution function). We then calculated the mean and SD in R_L and E_L over the 20 runs.

The second study explored the sensitivity to regional constriction and specifically the impact of localized constriction on lung mechanics. Simulations were performed after imposing a heterogeneous constriction pattern (μ = 50%, SD = 70%) on only specific regions of the lung. These included the apex area only, middle only, base area only, and the combined apex and mid regions. These studies will allow us to explore if there is a specific location(s) in the lung that is more sensitive to severe constriction patterns.

The third study examined the sensitivity to distributed constriction with varying degrees of heterogeneity and mean constriction, in different locations of the tree, while impacting the entire lung. Here we studied two cases. In case A, constriction severity and heterogeneity was highest in the apex, and then decreased as one traversed to the base of the lung (apex: μ = 50%, SD = 70%, middle: μ = 40% SD = 40%, and base: μ = 30%, SD = 30%). In case B the mean constriction remains the same but the SD decreases moving from the apex to the base (apex: μ = 50%, SD = 70%, middle: μ = 50% SD = 40%, and base: μ = 50%, SD = 30%).

The fourth simulation study was driven to identify constriction conditions that would match measurements of dynamic mechanical properties taken in an asthmatic subject with recently acquired ventilation distribution images in the same subject. Specifically, in a mild-moderate supine asthmatic, we measured R_L and E_L as in Ref. 7 before and after a methacholine challenge. PET images were also acquired on the same subject while supine by injecting a radioactive NN^{13} tracer gas intravenously while simultaneously acquiring images. At baseline, the images were acquired during a breath-hold of 40 s at mean lung volume and then during spontaneous breathing for 3 min. The protocol was repeated, after administration of methacholine. The degree of ventilation was quantified by how quickly the tracer gas washed out.[10]

From the PET data, we quantified ventilation distribution relative to anatomic location, while from the R_L and E_L data we quantified the impact of heterogeneous constriction on elevation in the level and frequency dependence of R_L and E_L. Simulations were performed to probe the mechanical response of the tree that would be consistent with both the measured lung impedance and the PET images. Three cases were created. In case 1, severe constriction in small airways ($d < 2$ mm) leading only to the cranial dorsal region (μ = 50%, SD = 70%) was considered while not constricting the remaining lung. This case was chosen because previous PET studies have revealed that the primary ventilation impairment occurred in these regions.[10] Case 2 imposed the constriction of case 1 combined with mild constriction (μ = 50%, SD = 40%) in the remaining small airways ($d < 2$ mm). The degree of constriction on the remaining portion of the lung was designed to not introduce additional airway closure to the lung but still require that these airways contribute to the overall mechanical response. Finally, case 3 imposed the constriction of case 1 plus constriction of the entire airway tree ($d < 2$ mm) with the same mean and spread (μ = 50%, SD = 70%). This case was selected to show the impact of excessive constriction, which is inconsistent with both the mechanics and PET data. Constriction was limited to airways with diameters <2 mm because simulation studies have suggested that increases in frequency dependence and levels of R_L and E_L in asthma derive largely from airway constriction in the peripheral airways.[2] In all cases, we compare the predicted R_L and E_L to the measured subject response.

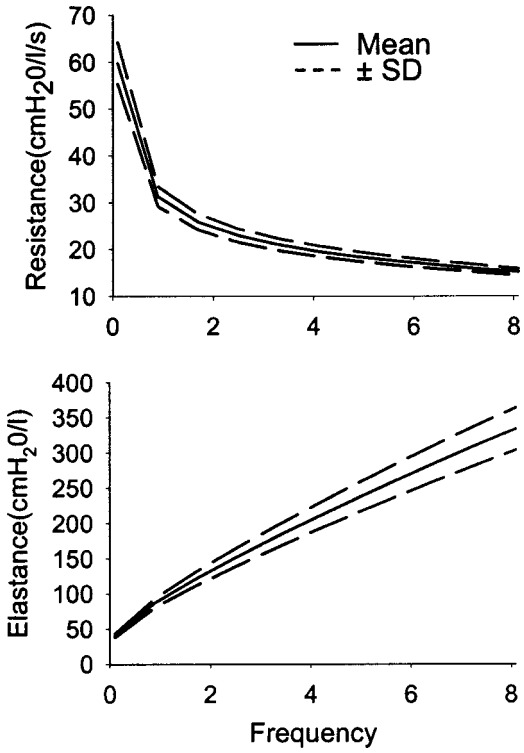

FIGURE 2. Average resistance (R_L) and elastance (E_L) for 20 runs of a Monte Carlo analysis using a Gaussian constriction probability distribution function (μ = 50% and SD = 70%).

RESULTS

Monte Carlo Analysis

The results from our first study using Monte Carlo analysis demonstrated that after 20 different random draws on the Gaussian distribution function, the variability in R_L and E_L was only about ±10% of the mean (Fig. 2). Thus, we may use the same random seed for each of our simulations and assume that R_L and E_L will be at most ±10% of the average.

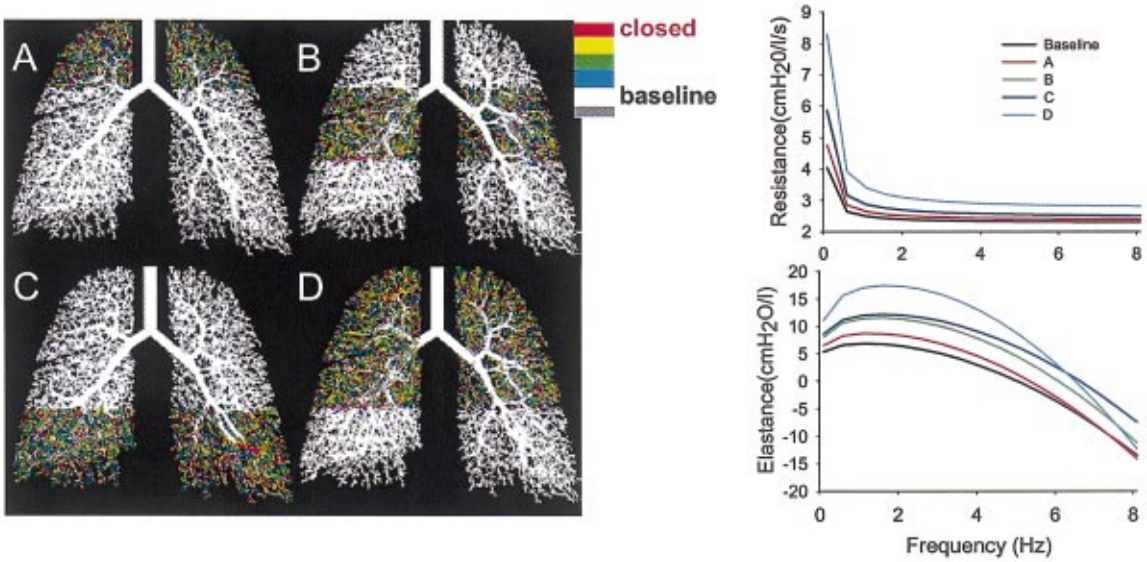

FIGURE 3. Impact of regional constriction on lung mechanics after imposing the same degree of constriction (μ=50%, SD=70%) in specific regions of the lung (A) apex, (B) middle, (C) base, and (D) apex and middle.

Regional Constriction

The mechanical responses of the tree at baseline and after affecting only a specific region in the lung are shown in Fig. 3. The dynamic response of the tree at baseline is consistent with published experimental data as well as simulated healthy mechanics from previous morphometric models.[2,7] The color bar describes the degree of constriction in each branch where white branches are diameters that remained at baseline lengths, and each color preceding white represents an increase of 20% in the severity of constriction. Thus, red branches are equivalent to 100% diameter reduction. The focus here was on how localized constriction in the lung affected mechanics. In all cases, affecting only a specific region of the lung had a relatively minor impact on mechanics especially when compared to affecting the entire lung. In particular, Z_{in} was least sensitive to regional constriction when changes were localized to the apex region. In short, Z_{in} is relatively insensitive to significant and heterogeneous constriction that is localized to one third or less of the lung in a specific region, e.g., apex and middle (Fig. 3).

Distributed Constriction

In Fig. 4, we evaluate whether varying degrees of mean constriction and heterogeneity in the lung impact lung mechanics. When a mild degree of constriction was applied to the middle and base of the lung, the mean level of R_L and E_L and frequency dependence were elevated from baseline (case A). However, by increasing the spread of constriction, we increased the probability of random airway closure and found that a significant fraction of the lung must have a high mean and spread in constriction in order to express whole lung measures reflective of heterogeneity in function (case B).

Image Guided Constriction

Analysis of the PET data revealed (Fig. 5) that the amount of tracer remaining in the alveoli at the end of washout at baseline was minimal. While in contrast, a substantial amount of tracer remains in a significant portion of the lung post challenge. In particular we observe that at least 17% of the lung has 80% or more of its tracer activity remaining after washout suggesting that 17% of the lung is communicating little or not at all with the airway opening because the alveoli are located behind closed airways. This suggests we need to significantly reduce communication to ~17% of the alveoli, located mainly in the cranial dorsal region, while matching R_L and E_L.

Three constriction simulations were performed. First, we applied a mean constriction of 50% with SD of 70% on only the cranial-dorsal portion of the airway tree. Figure 6 depicts a substantial amount of constriction, with airways that are closed in red or nearly closed in yellow. The total number of airways that are affected is about 5000 out of a total of about 50,400 airways in this particular tree. This case, then, placed constriction only in the cranial-dorsal region and we calculated that as a consequence 20% of the alveoli in this region were distal to at least one closed airway, and hence not ventilated. Hence, a ventilation defect consistent with the PET image was established (quantitatively and in location). Me-

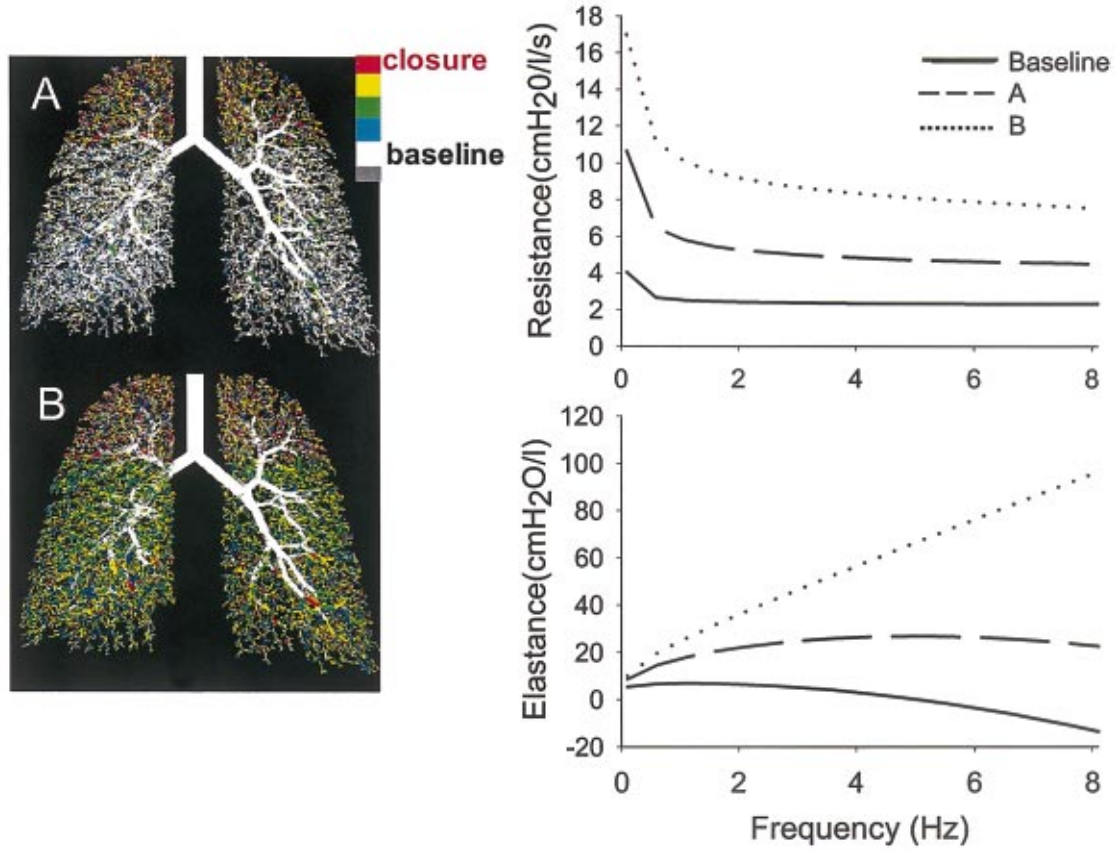

FIGURE 4. Impact of distributed constriction on lung mechanics. Case A: apex: $\mu = 50\%$, SD = 70%, middle: $\mu = 40\%$, SD = 40%, and base: $\mu = 30\%$, SD = 30%. Case B: apex: $\mu = 50\%$, SD = 70%, middle: $\mu = 50\%$, SD = 40%, and base: $\mu = 50\%$, SD = 30%.

chanically (Fig. 6), however, the impact was small and the R_L and E_L are only slightly elevated from baseline and far from measured data.

For the second simulation (case 2), we retained the same constriction pattern in the cranial dorsal region as in case 1, but now also induce constriction on the lower portion of the lung with the same mean ($\mu = 50\%$) but less heterogeneity (SD = 40%). The illustration of this constricted tree (Fig. 6) reveals mostly blue and green branches, which indicate milder constriction and virtually no additional airway closures (i.e., ventilation defects) from those occurring in case 1. Mechanically the impact was to increase R_L and E_L and cause both to show more frequency dependence (Fig. 6). By applying these two distinct constriction patterns, we now remain consistent with the ventilation defects observed in the PET images while simultaneously predicting an R_L and E_L that are consistent with measured mechanical data.

Finally, we can contrast case 2 with simulation case 3 which imposes a much larger standard deviation (SD = 70%) on the bottom part of the lung than case 2, while retaining the same mean constriction ($\mu = 50\%$). First, this created substantial additional airway closures in the bottom half of the lung (Fig. 6), which would create ventilation defects far in excess than observed in the PET data and in anatomic locations that are inconsistent with these data as well. Also, there is now a severe impact on the mechanics that is well in excess of measured R_L and E_L data (Fig. 6).

DISCUSSION

The emergent biomechanical properties and static and dynamic behavior of physiological systems derive from a complex relationship between structure and living conditions. Understanding this relationship in healthy and pathological conditions is greatly aided by synthesizing experimental data with mathematical modeling. The models can be used either to interpret data (which often involves systems identification) or to predict behavior (e.g., to develop a hypothesis and guide experiments). In either case, clearly the more structurally and mechanistically realistic the model is, the more powerful the process. Until recently, in the field of lung physiology, the process has been of limited utility. Models were primarily comprised of lumped properties with no explicit cor-

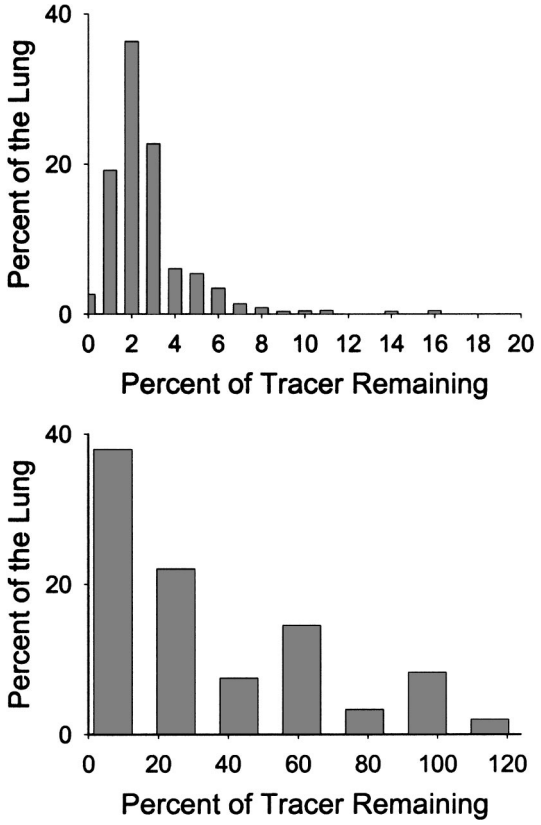

FIGURE 5. Histogram of percent of lung containing distinct percent tracer that remains at the end of washout pre(top) and post(bottom) methacholine challenge in one asthmatic using PET. Bin sizes were different for pre- and postchallenge. Note that all portions of the lung contain approximately 10% or less of original tracer premethacholine.

relation to the anatomy of biomechanical properties. Some recent studies have hinted at the possibility of a new generation of models. Computational power has recently permitted function to be predicted in airway tree models that are statistically and morphometrically consistent with a real human lung. These models have already provided new insights into structure-function relationships in healthy versus asthmatic lungs. They have suggested how different patterns of airway constriction likely contribute to the severity of an asthmatic response.[2] While these models are anatomically consistent, they are not anatomically explicit (i.e., there is not a one to one correlation between airways and alveoli in the model and an explicit airway or acinus in a 3D lung). We recognize, however, that imaging technologies that provide explicit anatomic details and loci of alterations in function are advancing in parallel with advances in computational capacity. To this end, we introduced function into a 3D model which allows specific control of anatomic regions, and tested how the model predictions compare with ventilation images obtained from PET and measurements of dynamic mechanical function.

Model Limitations

The scope of this paper was to present the concept of how physically and anatomically particular changes in the airway tree might alter lung function. Previous lung models have been unable to answer some of these questions because they were limited to one dimension and could not relate specific anatomic locations to specific locations in the airway tree. The 3D tree that we used in this modeling study was based on the model described by Kitaoka *et al.*[8] While this model accurately describes many of the anatomical contours of the lung and the amount of fluid flow delivered to each branch there are still some inconsistencies with this model. In fact, Tawhai *et al.* pointed out that the Kitaoka tree model is more asymmetrical than the actual human lung and is not strictly based on actual images of the lung.[18] In principal, our algorithm and approach could easily be applied to the anatomic model of Tawhai as well.

Our model, which has integrated the prediction of dynamic lung properties using the Kitaoka tree model, does not extend to the realm of computational fluid dynamics for more explicit predictions of time-domain gas transport. That is, the model has not yet been used to predict fluid streamlines or the consequence of turbulent flow on aerosol deposition in the airways since flow is assumed to be laminar throughout the lung. Hence, the current model is most relevant to predict phenomena associated with low peak flow conditions. Likewise, this model would be unable to predict the details of the large inhomogeneous ventilation distributions that are observed after provocation with histamine because the small airways that are affected are located proximal to the acini where flow is assumed to be diffusive.[20] Other than in the physical design of the model, the impact of branching angle on airway mechanics is also never introduced into our computations. Finally, we have not yet advanced the algorithm to predict standard measures of lung function (e.g., FEV_1 and FVC). However, in principal, this can be incorporated and earlier efforts by our group based on the Horsfield model could be extended to the 3D models as well.[16]

New Insights

We have presented two potential uses for the model. First, we predicted the sensitivity to explicit forms of potential constriction patterns. With explicit clarity, these simulations show that severe mean and heterogeneity of peripheral airway constriction confined to a single location in the lung (apex, mid, or base) generally will not manifest itself in substantial alterations in whole lung properties as measured from the airway opening (Fig. 3). Not until 2/3 of the peripheral airways throughout the lung are affected will one detect major increases in the levels and frequency dependence of R_L and E_L. This is

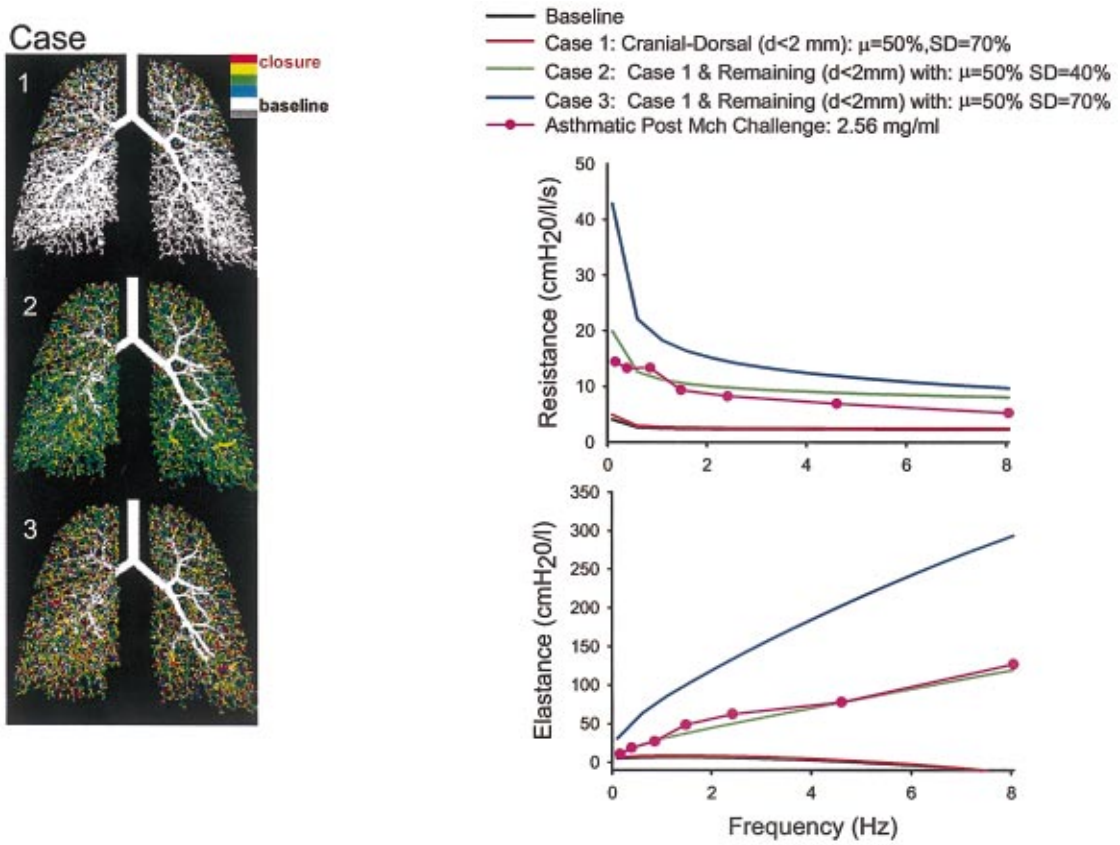

FIGURE 6. General attempt to match subject specific mechanical and PET measurements. Predicted resistance (R_L) and elastance (E_L) for three constriction cases with varying constriction μ and SD and subject postchallenge data are shown (right). Color coded constriction patterns for each respective case are shown on the left. Case 2 matches best with the subject post challenge data.

in accord with the notion that the lung is fairly resistant in function against localized constriction. Stated conversely, when measured R_L and E_L are abnormal, it is likely that significant constriction has occurred throughout the entire airway tree, and not confined to a small anatomic region. Similarly, once constriction does occur throughout the tree, the resulting impact on R_L and E_L is dependent on the combined impact of the mean level and heterogeneity of the constriction pattern (Fig. 4) and increased frequency dependence of these properties reflects heterogeneities capable of inflicting airway closures throughout the airway tree. We can contrast these findings to those implied from our previous morphometric models.[2,11] In those models we found that only a small percentage (~10%) of the peripheral airways needed to be highly constricted to cause significant changes in R_L and E_L. But, as with the 3D model, these 10% could not be localized in a single sector of the Horsfield tree. Rather, they had to be randomly occurring throughout the entire airway tree such that the input impedance along virtually all pathways from the airway opening to any arbitrary alveolus is increased.

The second presented application of the model was in the context of image-assisted modeling with the goal of advancing our understanding of how changes in lung structure alter function (Fig. 6). Our presentation here was strictly anecdotal and included to simply introduce the concept. In our one example subject we measured substantial elevations in R_L and E_L simultaneously with PET imaging data indicative of a ventilation defect in ~20% of the alveoli confined primarily to the cranial-dorsal region of the lung. Recall that the earlier sensitivity analysis studies predicted that significant changes in R_L and E_L occur only when a substantial portion of the lung is affected. Hence, it was not surprising that in order to match both the mechanics and the PET data we had to impose a substantial mean and heterogeneous constriction to the cranial-dorsal regions in the model while also imposing a substantial mean but less heterogeneous constriction to the remaining airways. The implication is that the methacholine did, in fact, affect the entire airway tree, and that the most severe constrictions leading to airway closures occurred in a more confined region. Also, it appears that the appropriate ventilation

and mechanical defects could be attained by severe constriction or closure of many small airways in the cranial-dorsal region rather than a few larger airways leading to this region (while constricting the remaining small airways less heterogeneously).

Limitations of Image-Assisted Modeling

It is certainly premature to overly interpret our one example of image-assisted modeling. Several challenges remain before this approach can be validated and exploited for explicit input on structure-function relations. For example, in our example we localized defects in lung anatomy by identifying ventilation dropouts in the lung after broncho-constriction with PET images. While the images obtained presented us with detail about ventilation in the lung, the PET data set was restricted to a 4 in. portion of the lung. Due to the limitations of the PET camera, in that study we did not scan the entire lung structure and could not quantify function in the very upper and lower portions of the lung. Modern PET cameras will be able to image a much larger fraction of the whole lung. Another potential imaging modality that may be used to provide information about structural defects after broncho-constriction is hyperpolarized magnetic resonance imaging (MRI).[1] Hyperpolarized MRI would provide us with information about what size airways are closing and their specific locations relative to the trachea. However, to date, quantifying changes in airway size is difficult and results are not easy to reproduce.

A second limitation to our particular example is that we simply provided a statistical matching of localized ventilation impairment but not a strict one–one mapping as observed in the images. That is, we identified a general location, i.e., cranial dorsal region, of severe ventilation defects in the PET images and generated a constriction pattern with approximately the same percentage of alveoli not communicating with the airway opening. However, the fidelity of the process would be improved if constriction in the airway tree model was confined to those airways leading to the explicit nonventilated alveoli as identified in the PET data. Such explicit control is possible algorithmically, but would require imaging data better matched to the entire lung in the thorax, rather than just a 4–8 in. segment. Because the 3D model is a generic human lung model, one would have to make a new airway tree on a personalized basis to match specific airways in the model to the imaging data, although, the Monte Carlo analysis implies that this is likely not necessary.

Summary

We have advanced a 3D model for predicting the impact of explicit anatomic structure on dynamic lung function. This modeling approach can be used to provide new insight on the sensitivity of whole lung measurements to the severity, location, and extent of particular injury or pathology. In principle, deeper insight on the impact of other phenomena, such as wall thickening associated with inflammation, can be attained. We have also introduced the concept of image-assisted modeling. Here imaging information revealing explicit anatomic information and defects can be incorporated to predict the impact on mechanical function and then compared to sensitive experimental measures of this function. Certainly substantial challenges in imaging resolution and data comparisons remain before this approach can be fully exploited. When faced with a patient with both measured degradation in whole lung mechanical function and images identifying anatomically specific degradation in ventilation function, one ultimate goal would be personalized predictions of which airways may or may not be constricted and by how much.

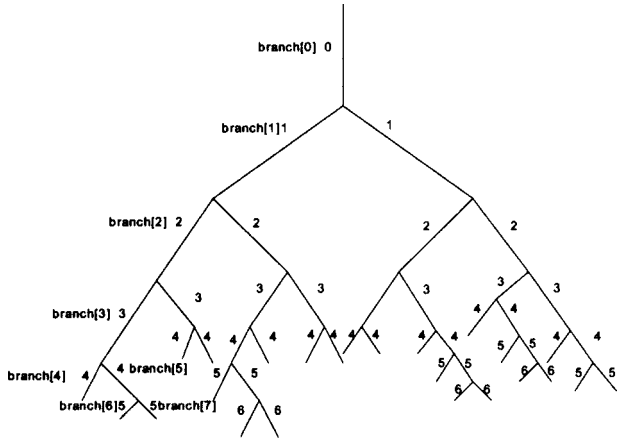

FIGURE 7. Example airway tree figure used for calculation of lung impedance (Z_L). Generation numbers are shown next to the corresponding branch. branch [#] indicates the location of each branch in the data file.

ACKNOWLEDGMENTS

This work was supported by NIH Grant Nos. HL62269-02 and HL68011-01 and by NSF Grant No. BES0076818.

APPENDIX

In Fig. 7, we show an example of an airway tree, with corresponding generations for each airway segment. A generation is defined as the number of bifurcations from the trachea, needed to reach an airway. Each airway segment is assigned a branch number (branch [#]), which includes the properties specific to that airway, i.e., generation number, diameter, and length. Branch numbering begins at the trachea (branch [0]) and increases as one proceeds along the left pathway. Once a terminal airway

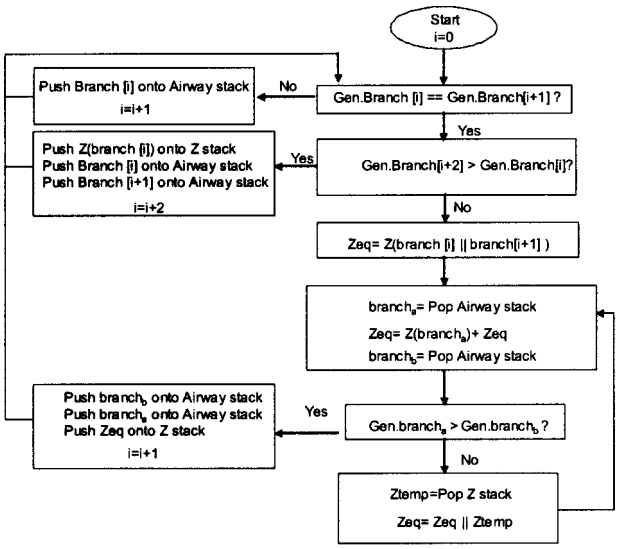

FIGURE 8. Flow chart for traversing through airway tree.

is reached, incremental branch numbering continues along the sister branch of the terminal airway. Note, although we show a two-dimensional airway tree, each branch has its own unique three dimensional coordinate.

To begin calculation of Z_{in} (Fig. 8) we start at the trachea, which is the first branch in the airway tree file. Initially, $i=0$, hence, branch [0] is the trachea and branch $[i+1]$ is the left daughter branch (generation 1). We check to see if the generations of the two branches are equivalent. Since this is not true, the airway properties of the trachea (branch [0]) are pushed onto the airway stack. The array index is incremented ($i=i+1$) and we begin again comparing the generations of branch $[i]$ and branch $[i+1]$, in this case branch [1] and branch [2], respectively. The process of checking to see if the generation of the current branch $[i]$ is equivalent to the generation of branch $[i+1]$ and pushing branch $[i]$ onto the airway stack, continues until the two are equal, in which case we may take one of two paths. In Fig. 7, this process continues until we are at branch [4] and branch [5]. First, the generation of branch $[i+2]$ (branch [6]) is checked to see if it is greater than branch [4]. This indicates that branching will continue along branch [5], and the impedance of branch [4] is stored and pushed onto the Z_{stack}. The airway properties of branch [4] and branch [5] are pushed onto the airway stack. i is then incremented such that the branch [6] is the current branch and branch [7] is the next branch. The algorithm then proceeds as before to check if the generation of branch $[i]$ is equivalent to branch $[i+1]$. Once again we stop when we reach two terminal airways (branch [6] and branch [7]).

The second path we may take when we have found that the generation of branch $[i]$ is equal to branch $[i+1]$ is to combine the impedances of the two branches in parallel, as they represent a pair of terminal branches with a common parent branch. In Fig. 7 this occurs for the first time at branch [6] and branch [7]. Airway stack is popped to retrieve the airway branch properties of the common parent branch (branch $[5]=\text{branch}_a$). The impedance of the branch_a is computed and added in series with the parallel combination of the terminal branches for Z_{eq}. The airway stack is then popped again (branch $[4]=\text{branch}_b$) and the generation of this branch is compared with that of branch_a.

If we compare branch_a and branch_b, and found their generations were the same, which is the case in our example, we pop the Z_{stack} to retrieve the equivalent impedance of looking into branch_b i.e., impedance of branch [4] and combine it in parallel with the current Z_{eq} for a new Z_{eq}. We then pop the airway stack to retrieve branch [3] and added in series to Z_{eq}. The airway stack is popped again for branch $[2]=\text{branch}_b$ and compared to the generation of branch_b. The generation of branch_a is greater than that of branch_b, so branch_b and branch_a are both pushed back onto the airway stack because. The current Z_{eq} is also pushed onto Z_{stack}, i is incremented and we continue to proceed down the tree until we reach two consecutive branches with the same generation.

This stack-based algorithm is continued until the current index i is equal to the number of branches in the airway tree in which case $Z_{\text{eq}}=Z_{\text{in}}$. By traversing the tree in this manner, we have the capability of computing the impedance of each branch individually and thus can incorporate anatomic changes such as heterogeneous broncho-constriction and ASM shortening into our simulation studies.

REFERENCES

[1] Altes, T., P. L. Powers, J. Knight-Scott, G. Rakes, T. A. Platts-Mills, E. E. de Lange, B. A. Alford, J. P. Mugler III, and J. R. Brookeman. Hyperpolarized 3He MR lung ventilation imaging in asthmatics: Preliminary findings. *Magn. Reson. Imaging* 13:378–384, 2001.

[2] Gillis, H. L., and K. R. Lutchen. Airway remodeling in asthma amplifies heterogeneities in smooth muscle shortening causing hyperresponsiveness. *J. Appl. Physiol.* 86:2001–2012, 1999.

[3] Gillis, H. L., and K. R. Lutchen. Convective ventilation distribution during heterogeneous constriction in human lungs assessed via morphometric modeling. *Ann. Biomed. Eng.* 27:14–22, 1999.

[4] Hantos, Z., B. Daroczy, B. Suki, S. Nagy, and J. J. Fredberg. Input impedance and peripheral inhomogeneity of dog lungs. *J. Appl. Physiol.* 72:168–178, 1992.

[5] Horsfield, K. Morphometry of airways. Handbook of Physiology. American Physiological Society, 1986, Chap. 7.

[6] Horsfield, K., G. Dart, D. E. Olson, F. Filley, and G. Cumming. Models of the Human Bronchial Tree. *J. Appl. Physiol.* 31:207–217, 1971.

[7] Kaczka, D. W., E. P. Ingenito, B. Suki, and K. R. Lutchen. Partitioning airway and lung tissue resistances in humans: Effects of bronchoconstriction. *J. Appl. Physiol.* 82:1531–1541, 1997.
[8] Kitaoka, H., R. Takaki, and B. Suki. A three-dimensional model of the human airway tree. *J. Appl. Physiol.* 87:2207–2217, 1999.
[9] Kuwano, K., C. H. Bosken, P. D. Pare, T. R. Bai, B. R. Wiggs, and J. C. Hogg. Small airway dimensions in asthma and in chronic obstructive pulmonary disease. *Am. Rev. Respir. Dis.* 148:1220–1225, 1993.
[10] Layfield, J. D. H., R. S. Harriss, G. Musch, M. F. Vidal Melo, R. J. Callahan, A. J. Fischman, K. R. Lutchen, and J. G. Venegas. Measurement of gas trapping during bronchoconstriction. *Am. J. Respir. Critical Care Medicine* 163:A422, 2001.
[11] Lutchen, K., A. Jensen, H. Atileh, D. W. Kaczka, E. Isreal, B. Suki, and E. P. Ingenito. Airway constriction pattern is a central component of asthma severity: The role of deep inspirations. *Am. J. Respir. Critical Care Medicine* 164:207–215, 2001.
[12] Lutchen, K. R., and H. L. Gillis. Relationship between heterogeneous changes in airway morphometry and lung resistance and elastance. *J. Appl. Physiol.* 83:1192–1201, 1997.
[13] Lutchen, K. R., J. R. Everett, and A. C. Jackson. Impact of frequency range and input impedance on airway-tissue separation implied from transfer impedance. *J. Appl. Physiol.* 74:1089–1099, 1993.
[14] Mandelbrot, B. B. The Fractal Geometry of Nature. San Francisco, CA: Freeman, 1982.
[15] Murray, C. D. The physiological principle of minimum work. *Proc. Natl. Acad. Sci. U.S.A.* 12:207–214, 1926.
[16] Polak, A. G., and Lutchen K. R. Forced expiration from heterogeneous lungs—A model study. *Am. J. Respir. Crit. Care Med.* 163, 2001.
[17] Suki, B., R. H. Habib, and A. C. Jackson. Wave propagation input impedance and wall mechanics of the calf trachea from 16–1,600 Hz. *J. Appl. Physiol.* 75:2755–2766, 1993.
[18] Tawhai, M. H., A. J. Pullan, and P. J. Hunter. Generation of an anatomically based three-dimensional model of the conducting airways. *Ann. Biomed. Eng.* 28:793–802, 2000.
[19] Thorpe, C. W., and J. H. T. Bates. Effect of stochastic heterogeneity on lung impedance during acute bronchoconstriction: A model analysis. *J. Appl. Physiol.* 82:1616–1625, 1997.
[20] Verbanck, S., D. Shuermans, A. Ban Muylem, M. Paiva, M. Noppen, and W. Vinchken. Ventilation distribution during histamine provocation. *J. Appl. Physiol.* 83:1907–1916, 1997.
[21] Weibel, E. R. Morphometry of the Human Lung. New York: Academic, 1963.